Journal of Non-Crystalline Solids: X 5 (2020) 100044

Contents lists available at ScienceDirect

Journal of Non-Crystalline Solids: X

journal homepage: www.journals.elsevier.com/journal-of-non-crystalline-solids-x

Correlation between the optical bandgap and the monohydride bond density of hydrogenated amorphous silicon

Jonathan Steffens*, Johannes Rinder, Giso Hahn, Barbara Terheiden

University of Konstanz, Department of Physics, 78457 Konstanz, Germany

ARTICLE INFO

Keywords:
Hydrogenated amorphous silicon
Optical bandgap
Monohydride bond density
Fourier-transform infrared spectroscopy
Spectroscopic ellipsometry

ABSTRACT

In this study, a variation of the substrate temperature during plasma enhanced chemical vapor deposition of hydrogenated amorphous silicon is reported, which revealed a local minimum of the optical bandgap. It is shown, that the silicon monohydride bond density is more appropriate to describe this dependency than the commonly discussed layer properties hydrogen concentration and structural disorder. Furthermore, a high silicon monohydride bond density regime is suggested, in which the optical bandgap is independent of the bond density. This hypothesis explains previously published constant optical bandgaps under variation of the hydrogen concentration and structural disorder.

1. Introduction

Hydrogenated amorphous silicon (a-Si:H) layers are successfully implemented in photovoltaic applications [1]. For each purpose it is important to know and control the structural, optical and electronic properties of the specific layer. Even if these properties have been investigated for more than forty years, there are still unresolved discussions ongoing, especially about the fundamental layer property determining the optical band gap E_{gap} of a-Si:H. One line of publications argues for the structural disorder with a monotonic decreasing relation (disorder increase, E_{gap} decrease) [2,3] and another line for the hydrogen concentration c_H with a monotonic increasing relation (c_H increase, E_{gap} increase) [4,5]. The difficulty of this discussion lies in the interdependency of both properties [6,7]. Therefore, some authors concluded that neither the hydrogen concentration nor the structural disorder influences E_{gap} in an isolated way [8,9]. The authors in [9] found from a simulation study, that the hydrogen concentration influences E_{gap} only if the a-Si:H is undersaturated with hydrogen, while E_{gap} reaches a constant value independent of the hydrogen concentration for saturated a-Si:H.

In the present study, the influence of the substrate temperature during deposition on E_{gap} is investigated, as this parameter affects both the hydrogen concentration and the structural disorder. It is shown that both quantities are necessary to describe an observed local minimum of E_{gap}, while the silicon monohydride (Si-H) bond density describes this dependency alone. Previous studies investigating the influence of the deposition temperature revealed monotonic decreasing E_{gap} values [4,10] or constant E_{gap} values with increasing deposition temperature, even if the structural disorder was reduced significantly [11].

In order to support the ongoing discussion a high Si-H bond density regime is suggested, which explains the above mentioned constant E_{gap} values in [11] and it does also support the discussion about the E_{gap} values independent of the hydrogen concentration for saturated a-Si:H in [9].

2. Experimental

2.1. Deposition

a-Si:H layers were plasma-enhanced chemical vapor deposited (PECVD) on chemically polished boron doped silicon floating zone wafers (~1 Ωcm) with a thickness of ~230 µm using a direct plasma reactor (PlasmaLab 100 from Oxford Instruments) immediately after a short dip in hydrofluoric acid solution (5%) to remove the native silicon oxide. All plasma parameters were kept constant except for the substrate heater set temperature (in the following referred to as deposition temperature), which was varied between 100 °C and 400 °C (see Table 1). Since the deposition duration was kept constant and the deposition rate increases with increasing deposition temperature [12], the resulting layer thickness was also increased. Additionally, the atomic hydrogen concentration is reduced with increasing deposition temperature, which was previously measured on similar samples using resonant nuclear reaction analysis (NRA) [13]. This technique determines the hydrogen concentration by measuring the γ-ray yield from

* Corresponding author.
E-mail address: jonathan.steffens@uni-konstanz.de (J. Steffens).

https://doi.org/10.1016/j.nocx.2020.100044
Received 11 November 2019; Received in revised form 10 January 2020; Accepted 11 January 2020
Available online 13 January 2020

Table 1
PECVD deposition parameters. The total deposition duration is the sum of ignition step duration and deposition duration. The flux ratios are defined as $R_x = [X]/([X] + [SiH_4])$.

Parameter	Value
Heat up duration	10 min
Power	10 W
Pressure	1 Torr
R_H	0.5
R_{Ar}	0.95
Electrode distance	22 mm
Ignition step	20 W, 10 s
Deposition duration	1500 s
Deposition temperature	100–400 °C

a resonant nuclear reaction of ^{15}N ions with the hydrogen in the a-Si:H layer [14].

2.2. Spectroscopic ellipsometry

Layer thicknesses as well as the wavelength dependent refractive indices n and extinction coefficients k were determined by spectroscopic ellipsometry (SE) using a Vertical VASE Rotating Analyzer Ellipsometer (J.A. Woollam Co., Inc.) in the spectral range of 240–2000 nm with a step width of 10 nm and 40 measurements per step at 70°, 75° and 80° incident angles. The evaluation was divided into two steps. First, a reference sample without an a-Si:H layer was measured by SE and a table of optical constants (n, k) was created with a so called point-by-point fit of pure crystalline silicon starting at the wavelength of 2000 nm down to 240 nm. Second, the measured ellipsometric parameters (Ψ,Δ) of each sample were fitted using the following three layer model:

1. Substrate: (n, k) table determined from the reference sample.
2. a-Si:H: standard Tauc-Lorentz parametrization [15,16].
3. Roughness: simulated by an effective medium approximation of 50% underlying layer material and 50% voids [17].

The resulting wavelength dependent extinction coefficient $k(\lambda)$ was transformed into the absorption coefficient via $\alpha(\lambda) = 4\pi k/\lambda$, which allows to extract the Urbach tail width E_0 [2] with a fit in the region of $10^1\ cm^{-1} < \alpha < 5{\cdot}10^3\ cm^{-1}$. For amorphous semiconductors, the optical bandgap is not clearly defined due to the continuous decay of the band tail density of states [12]. However, in the literature the term optical bandgap usually refers to the value obtained by the so called "Tauc-plot" analysis [18], which was also applied in the present study to extract the optical bandgap value $E_{gap,tauc}$. As comparison, also the optical bandgap $E_{gap,fit}$ from the Tauc-Lorentz parametrization of the SE fit was considered.

The uncertainties of the optical constants were determined starting from a Gaussian uncertainty propagation of the Tauc-Lorentz parametrization with the errors of the fit parameters as input values. For $E_{gap,fit}$ the uncertainty is the SE fit parameter error, and for E_0 and $E_{gap,tauc}$ the uncertainties were obtained by the error of the fits described in the corresponding references [2, 18].

2.3. Fourier-transform infrared spectroscopy

Hydrogen bonding states, hydrogen concentration c_H and the microstructure of the layers were analyzed by Fourier-transform infrared spectroscopy (FT-IR) using a commercial tool (Vertex 80 from Bruker Optics) in the spectral range from 400 to 2500 cm^{-1} with a resolution of 4 cm^{-1} averaging over 50 spectra. After a polynomial baseline correction of the absorbance spectrum and the subtraction of a reference sample spectrum, the wavenumber dependent effective

Table 2
Analyzed silicon-hydrogen absorption bands in a-Si:H with underlying absorption peaks and corresponding bonds.

Absorption band	Spectral range (cm^{-1})	Peak (cm^{-1})	Bond	Ref.
Wagging	530–740	640	Si-H / $Si-H_2$	[19]
Bending	820–940	840	$Si-H_2$ pairs / $(Si-H_2)_n$ chains	[19]
		880	Isolated $Si-H_2$	[19]
Stretching	1900–2180	2000	Si-H	[20]
		2080	$Si-H_2$	[20]

absorption coefficient

$$\alpha_{eff}(\omega) = \frac{A(\omega)}{d \cdot \log_{10}(e)} \tag{1}$$

was determined with the baseline and reference corrected absorbance $A(\omega)$ and the layer thickness d determined by SE. From this the absorption strength of each absorption peak was determined by integrating each peak via

$$I_x = \int_{400\ cm^{-1}}^{2500\ cm^{-1}} \frac{\alpha_{eff}(\omega)}{\omega} d\omega \tag{2}$$

where x is the literature absorption peak position and $\alpha(\omega)$ is the corresponding Gauss curve from a standard two-Gaussian fit in the range of the corresponding absorption band (see Table 2). The uncertainty of each absorption strength was estimated by the difference between the absorption strength and the integrated Gaussian uncertainty propagation of the corresponding integrand of Eq. (2) with the 95% confidence intervals of the fit parameters as uncertainty input.

From these absorption strengths the corresponding bond density is calculated via

$$N_z = A_x \cdot I_x \tag{3}$$

with A_x experimentally determined proportionality constants $A_{2080} = 1.6{\cdot}10^{19}\ cm^{-2}$ and $A_{2000} \approx A_{2080} = 9.1{\cdot}10^{19}\ cm^{-2}$ [21]. z is either Si-H/$Si-H_2$ for $x = 640$, Si-H for $x = 2000$ or $Si-H_2$ for $x = 2080$. These bond densities can be divided by the silicon monocrystal bond density $n_{Si} = 5{\cdot}10^{22}\ cm^{-3}$ in order to obtain the hydrogen concentrations via

$$c_H = \frac{\sum N_i}{n_{Si}} \tag{4}$$

with a summation over all peaks of either the wagging or the stretching band.

In the present study, the bending and stretching absorption bands of silicon hydrogen bonds in a-Si:H were analyzed in depth, while the wagging band was only used for determination of the hydrogen concentration (see Table 2). For the bending band (820–940 cm^{-1}) it is assumed that the absorption peak at 840 cm^{-1} is a result of interactions between $Si-H_2$ pairs or $(Si-H_2)_n$ chains, whereas mostly isolated $Si-H_2$ bonds contribute to the absorption peak at 880 cm^{-1} [19]. Following the authors in [19] the ratio

$$Q = \frac{I_{840}}{I_{880}} \tag{5}$$

can be considered as indicator for microvoid formation, as the inner surfaces of such microvoids are assumed to be decorated by $Si-H_2$ bonds, which are then close enough to each other to build $Si-H_2$ pairs or $(Si-H_2)_n$ chains. Consequently, in a less ordered amorphous network with many microvoids the ratio Q should be higher than in a well-structured network with only few microvoids.

The stretching band (1900–2180 cm^{-1}) can be used for both the determination of the hydrogen concentration and as indicator for structural differences. Typically, the absorption peak at 2000 cm^{-1} is

attributed to silicon monohydride (Si-H) bonds and the peak at 2080 cm^{-1} to silicon dihydride ($Si-H_2$) bonds [22]. This clear attribution is constantly discussed in the literature [19,21,23,24] but it is sufficient for the purpose of this study. For the determination of c_H, the bond densities of both absorption peaks at 2000 cm^{-1} and 2080 cm^{-1} have to be summed up and then divided by the silicon atomic density of $\sim 5 \cdot 10^{22}$ cm^{-3} [21].

Another typical measure for structural differences is the microstructure factor [25].

$$R = \frac{I_{2080}}{I_{2000} + I_{2080}} \tag{6}$$

which is higher for a less structured amorphous network, since such a network offers more silicon atoms with two dangling bonds for $Si-H_2$ formation than a well-structured network. Also the above discussed decoration of microvoids by $Si-H_2$ bonds leads to a higher microstructure factor. Since the corresponding $Si-H_2$ bonds contribute to the absorption peak also if they are isolated, R should be basically independent of the hydrogen concentration. In contrast, the absorption peak at 840 cm^{-1} for the ratio Q only appears if the distance between two $Si-H_2$ bonds is sufficiently small, which clearly depends on the hydrogen concentration, i.e. at low hydrogen concentration Q could be small even if microvoids are present.

Table 3
Layer thicknesses d, Si-H bond density N_{Si-H} and $Si-H_2$ bond density N_{Si-H2} from Eq. (3).

Deposition temperature (°C)	d (nm)	N_{Si-H} (10^{21} cm^{-3})	N_{Si-H2} (10^{21} cm^{-3})
100	392 ± 1	4.90 ± 0.23	4.71 ± 0.20
150	489 ± 1	4.11 ± 0.18	3.58 ± 0.15
200	558 ± 1	3.52 ± 0.08	3.18 ± 0.07
250	618 ± 2	3.39 ± 0.06	2.59 ± 0.06
300	685 ± 2	3.48 ± 0.07	2.12 ± 0.08
400	747 ± 1	3.89 ± 0.10	1.33 ± 0.11

3. Results and discussion

3.1. Hydrogen concentration and structural disorder

Fig. 1a,b) show the wavenumber dependent absorption coefficients of all samples in the above specified ranges of the silicon hydrogen absorption bands. The layer thicknesses necessary for determination of the absorption strengths from Eq. (2) and the absorption strengths for each absorption peak are shown in Table 3. The layer thicknesses are in a range, where they might act as anti-reflective layer and cause interference oscillations in the FT-IR spectra. The effect was only observed for the samples deposited at 100–200 °C in a range of roughly 2–4% amplitude in the transmittance spectrum, which was considered for these samples as uncertainty on the fitted peak height.

In Fig. 1a,b) an obvious trend is observed for a decreasing overall

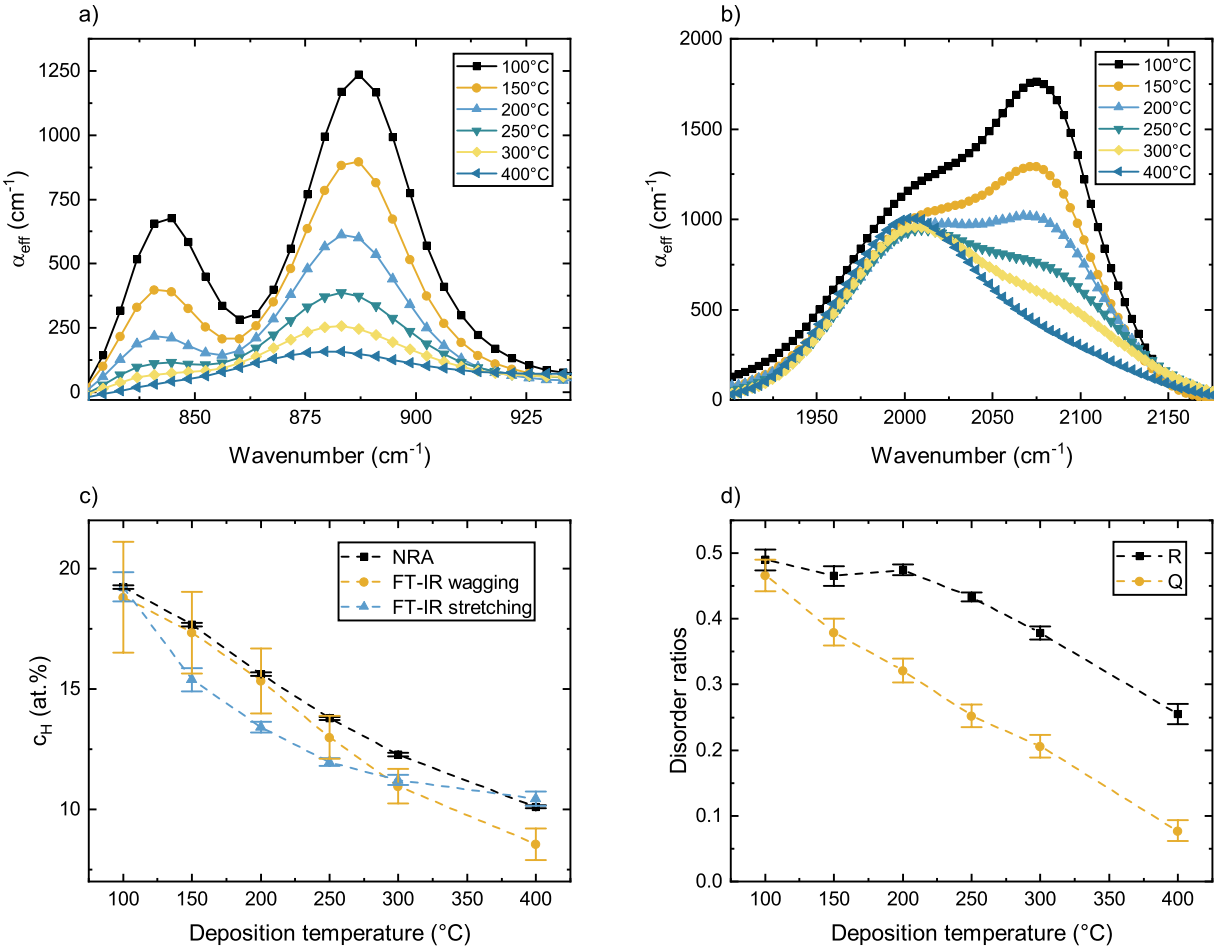

Fig. 1. FT-IR measured effective absorption coefficients for a) the bending and b) the stretching absorption band of hydrogen in a-Si:H. c) Hydrogen concentration determined from NRA measurements taken from [13] and from the FT-IR wagging and stretching band (Eq. (4)). d) Microstructure factor R and ratio Q according to Eqs. (5)–(6). Lines as guide for the eye.

absorption coefficient with increasing deposition temperature, which is due to a lower hydrogen concentration as depicted in Fig. 1c). The NRA data were published elsewhere [13] and due to the small error they act as reference for the FT-IR determined hydrogen concentrations. The hydrogen concentration derived from the FT-IR measurements (Eq. (4)) are up to ~2 at.% lower than the NRA measured concentrations, which could be a consequence of the fact that NRA measures the total hydrogen concentration, while FT-IR measures the bonded hydrogen only. Consequently, one could conclude the presence of trapped molecular hydrogen within the layers deposited at medium deposition temperatures in the range of 150–400 °C [26]. Nevertheless, irrespective of the method used for their determination, all hydrogen concentrations plotted in Fig. 1c) agree regarding the decreasing trend with higher deposition temperatures and the absolute value for each deposition temperature.

The microstructure factor R, estimated from the stretching band (Fig. 1a) and the ratio Q, estimated from the bending band Fig. 1b), show a similar decreasing trend with increasing deposition temperature Fig. 1d), which corresponds to a decrease in structural disorder. Even if the ratio Q is not necessarily a useful parameter for the disorder for low c_H as stated above, the trend can be trusted as it is confirmed by the microstructure factor R.

3.2. The microvoid volume fraction c_{void}

To investigate the structural disorder in more detail, the microvoid volume fraction c_{void} in the a-Si:H layers is introduced. The advantage compared to the disorder parameters R and Q is, that it is determined by a combination of the three independent measurement techniques SE, FT-IR and NRA.

Therefore, the wavelength dependent optical constants as obtained by the SE fit procedure described in Sec. 2.2 for all deposition temperatures are presented in Fig. 2. Over the whole spectrum there is a dependency of higher refractive index with higher deposition temperature, especially for the refractive index at 2000 nm (see Table 4). The only exception is the maximum value at roughly 275 nm for the sample with a deposition temperature of 200 °C. The increasing refractive index can be explained by the lowering of the hydrogen concentration with increasing deposition temperature as observed by the FT-IR analysis above (Fig. 1c) [8,27]. The extinction coefficient does not follow such a clear trend and will be discussed later.

From these SE results and the NRA determined hydrogen concentrations, the mass density of a-Si:H as function of the hydrogen concentration and the refractive index can be derived as described in [28]

Table 4
Refractive indices n_∞ at 2000 nm from SE, NRA measured hydrogen concentrations $c_{H,NRA}$ from [13] and a-Si:H densities $\rho_{a\text{-}Si:H}$ according to Eq. (7) for all deposition temperatures.

Deposition temperature (°C)	n_∞	$c_{H,NRA}$ (at.%)	$\rho_{a\text{-}Si:H}$ (g/cm^3)
100	3.148 ± 0.072	19.22 ± 0.08	2.077 ± 0.016
150	3.203 ± 0.073	17.67 ± 0.08	2.101 ± 0.017
200	3.272 ± 0.076	15.61 ± 0.07	2.131 ± 0.017
250	3.333 ± 0.080	13.77 ± 0.07	2.157 ± 0.014
300	3.404 ± 0.074	12.27 ± 0.07	2.183 ± 0.012
400	3.440 ± 0.071	10.10 ± 0.06	2.200 ± 0.020

$$\rho_{a-Si:H} = \left(\frac{n_\infty^2 - 1}{n_\infty^2 + 2}\right) \cdot \frac{3m_{Si}}{4\pi} \cdot \left[4\xi + \frac{c_H}{1 - c_H}(\alpha_{Si-H} - \xi)\right]^{-1} \tag{7}$$

with the refractive index n_∞ for $\lambda \to \infty$ approximated by the refractive index at 2000 nm from the SE measurements (see Table 4), m_{Si} the mass of a silicon atom, c_H the NRA measured hydrogen concentration from [13] (see Table 4), $\alpha_{Si\text{-}H} = 1.36{\cdot}10^{-24}$ cm^3 the Si-H bond polarizability approximated by the polarizability of a SiH_4 molecule [27] and $\xi = [(1-p)\alpha_{Si-Si,c-Si} + p\alpha_{Si-Si,a-Si}]/2$ with p the fraction of the amorphous phase, which is here set to 1 under the assumption of a fully amorphous material, so that the expression is simplified to $\xi = \alpha_{Si-Si,a-Si}/2$ with $\alpha_{Si\text{-}Si,a\text{-}Si} = 1.96{\cdot}10^{-24}$ cm^3 the polarizability of the Si-Si bond in the amorphous phase [28]. The resulting mass densities are depicted in Table 4.

From these a-Si:H mass densities and the stretching FT-IR absorption bond densities $N_{Si\text{-}H}$ and $N_{Si\text{-}H2}$ (Table 3), the authors in [20] established a method to determine the microvoid density

$$N_{void} = \frac{N_{Si-H2}^3 \cdot \rho_{Si}^2}{4\pi\rho_S^3\,[3(\rho_{Si} - \rho_{a-Si:H}) + 3m_H(N_{Si-H} + N_{Si-H2}) - m_{Si}N_{Si-H}]^2} \tag{8}$$

and the average microvoid diameter

$$D_{void} = \frac{2\rho_S\,[3(\rho_{Si} - \rho_{a-Si:H}) + 3m_H(N_{Si-H} + N_{Si-H2}) - m_{Si}N_{Si-H}]}{N_{Si-H2}\cdot\rho_{Si}} \tag{9}$$

under the assumption of a spherical void shape. $\rho_S = 7.83{\cdot}10^{14}$ cm^{-2} is the bonded H density on the inner surfaces of a microvoid, $\rho_{Si} = 2.33$ g·cm^{-3} the crystalline silicon mass density and m_H the mass of a hydrogen atom. The resulting void densities and diameters are similar to previously published results [20,29] and are presented in Fig. 3. The microvoid density decreases with increasing deposition

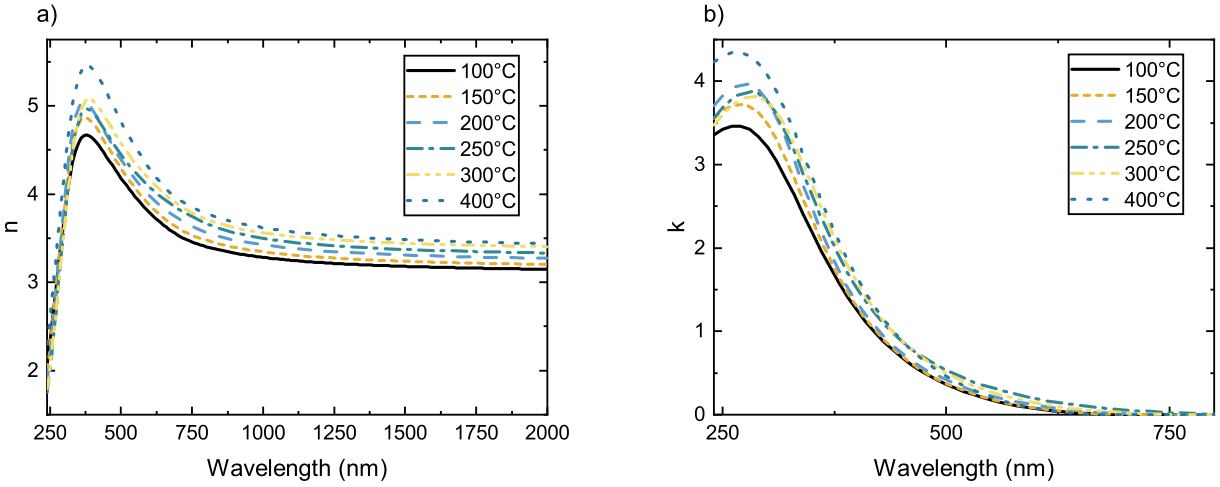

Fig. 2. Wavelength dependent optical constants as obtained by the SE fit procedure described in Sec. 2.2 for all deposition temperatures: a) refractive index n and b) extinction coefficient k.

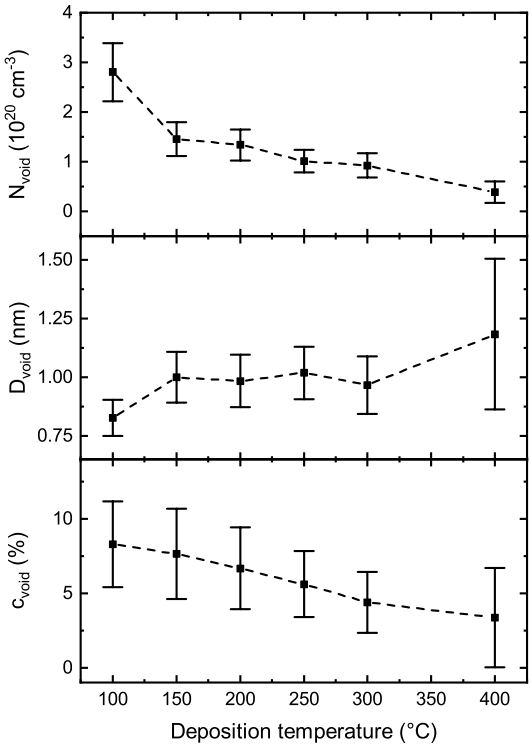

Fig. 3. Microvoid density N_{void}, microvoid diameter D_{void} and microvoid volume fraction c_{void} from Eqs. (8)–(10) as function of the deposition temperature. Lines as guide for the eye.

temperature, as it is expected from the decreasing structural disorder concluded from disorder ratios R and Q (Fig. 1d). Unexpectedly, the microvoid diameter increases at the same time. To resolve these reverse trends, the microvoid volume fraction

$$c_{void} = V_{void} \cdot N_{void} = \frac{4}{3}\pi\left(\frac{D_{void}}{2}\right)^3 \cdot N_{void} \tag{10}$$

is introduced and also presented in Fig. 3. c_{void} describes the volume fraction of microvoids in the a-Si:H material under the assumption of a spherical void shape. From Fig. 3 it is evident, that the volume fraction of microvoids decreases with increasing deposition temperature and hence it confirms the observation of decreasing disorder as concluded from the disorder parameters R and Q. Since c_{void} is determined by three independent methods (SE, FT-IR, NRA), it has more significance than R and Q, which were determined solely by FT-IR.

3.3. The optical bandgap E_{gap}

For the extinction coefficient no monotonic dependency on the deposition temperature was observed (Fig. 2b). As it is the basis for the determination of the optical bandgap, also for E_{gap} no monotonic dependency was found (Fig. 4a). With increasing deposition temperature, both optical bandgap values decrease significantly from above 1.75 eV at 100 °C up to a local minimum at 250 °C of below 1.5 eV and then increase again up to above 1.8 eV at 400 °C, which are similar to the values at 100 °C. The optical bandgap values from the Tauc-plot analysis $E_{gap,tauc}$ show much larger errors and so it is used in the following analysis as worst case approximation. The Urbach tail width follows an inverted trend with a maximum at 250 °C and so a linear correlation between E_0 and E_{gap} was observed as shown in Fig. 4b), which is in line with previous publications [2,30].

Previously published deposition temperature dependencies of E_{gap} did not show a local minimum as in the present study [4,11]. However, in [10] a similar local minimum was found in the deposition temperature range of 250–300 °C for the microstructure factor R and the Urbach tail width E_0, but not for E_{gap}.

In the case of post-deposition anneals, monotonic decreasing E_{gap} values were found for up to 350 °C [2] and 500 °C [31] during which hydrogen effusion is assumed to increase the structural disorder [12]. An important difference between their experiments and the experiments in the present study is, that the increase of the post-deposition annealing temperature decreases the hydrogen concentration and increases the structural disorder, while the increase of the deposition temperature in the present study decreases the hydrogen concentration (Fig. 1c), but at the same time also decreases the structural disorder as can be seen by the decrease of the disorder ratios R and Q (Fig. 1d). So for the variation of the deposition temperature, the hydrogen concentration and the structural disorder are assumed to be competing effects, which could give an explanation for the local minimum of E_{gap} as follows: For deposition temperatures < 250 °C the decrease of the hydrogen concentration is the dominating effect reducing E_{gap}, while for deposition temperatures > 250 °C the decrease in structural disorder becomes the dominating effect, which increases E_{gap}.

3.4. The correlation between the Si-H bond density and E_{gap}

Following the discussion in the literature, in this section the influence of the hydrogen concentration and the microvoid volume fraction c_{void} as measure for the structural disorder on E_{gap} are discussed in more detail. In Fig. 5a,b) E_{gap} is plotted versus both measures and it is evident, that, contrary to previous publications, neither the hydrogen concentration nor the structural disorder in terms of c_{void} is able to describe the dependency of E_{gap}, as the local minimum is also present in these plots.

In Fig. 5c) the Si-H bond density $N_{Si\text{-}H}$ is plotted versus the deposition temperature and a local minimum at roughly 250 °C is observable similar to the minimum of E_{gap} (Fig. 4a). Hence, the Si-H bond density follows the same trend as E_{gap} under variation of the deposition temperature and so it seems to be more appropriate to describe the variations of E_{gap} than the hydrogen concentration or the structural disorder. The reason for that might be, that the Si-H bond density is influenced by both factors: It decreases with decreasing hydrogen concentration under constant structural disorder, and it increases with decreasing structural disorder under constant hydrogen concentration. These are exactly the same dependencies claimed above for the explanation of the local minimum of E_{gap} via both the hydrogen concentration and the structural disorder. And indeed, in Fig. 5d) the Si-H bond density $N_{Si\text{-}H}$ is plotted versus E_{gap} and the local minimum of E_{gap} is not present. Instead, a monotonic increasing dependency is observed. The just raised hypothesis is supported by previously published monotonic increasing relationships between the Si-H bond density and E_{gap} [31,32].

The E_{gap} dependency on the Si-H bond density was fitted with the following exponential function

$$E_{gap} = E_{max} - a \cdot e^{-b \cdot N_{Si-H}} \tag{11}$$

with standard fit parameters a, b and an asymptotic maximum optical bandgap value E_{max} for high Si-H bond densities, in the following referred to as high Si-H bond density regime. Due to the three degrees of freedom and only six data points the fit should be only read as a rough estimate. Nevertheless, an interesting correlation to the above mentioned constant E_{gap} values in [11] is observed. Therein, the authors measured E_{gap} values of PECVD deposited a-Si:H in the range of 1.72–1.76 eV under variation of the deposition temperature between 50 and 200 °C. The fitted asymptotic value of E_{max} = 1.78 eV (Fig. 5d) in the present study is close to that range. Following this observation one could explain the constant E_{gap} values in [11] with the hypothesis that their layers have to be classified in the high Si-H bond density regime. This assumption of a high Si-H bond density is supported by the large

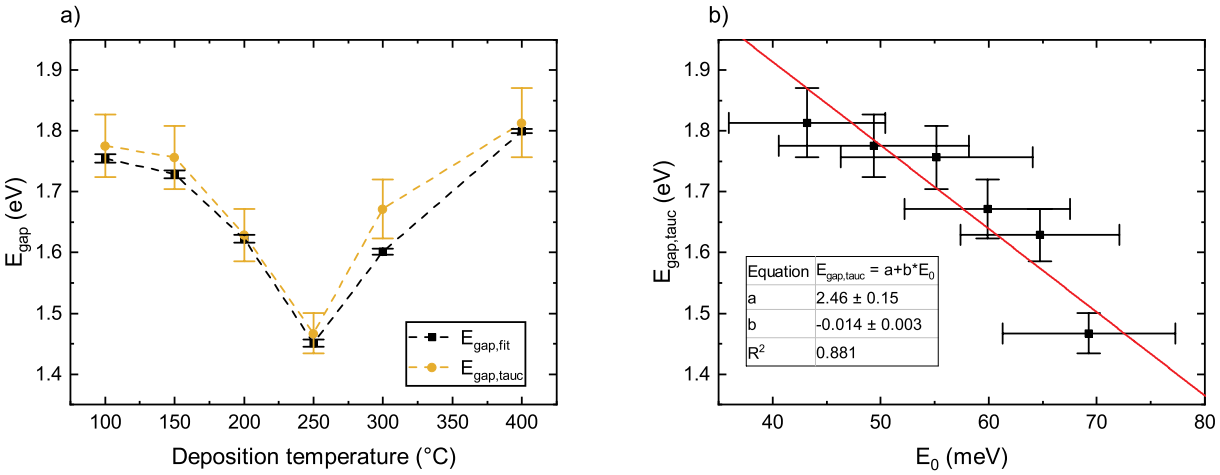

Fig. 4. a) Optical bandgaps $E_{gap,fit}$ and $E_{gap,tauc}$ as function of the deposition temperature. Lines as guide for the eye. b) Linear correlation between $E_{gap,tauc}$ and E_0. The straight line is a linear fit.

hydrogen concentration for a-Si:H layers deposited at temperatures < 200 °C (Fig. 1c). Also the simulated E_{gap} values in [9], which are independent of the hydrogen concentration for hydrogen saturated a-Si:H, are supported by this hypothesis. Saturated a-Si:H with a large hydrogen concentration could be considered to feature a high Si-H bond density and hence should also be classified in the high Si-H bond density regime, leading to the observed constant E_{gap} values.

4. Conclusions

It was shown that both the hydrogen concentration and the structural disorder are necessary to describe the observed local minimum of

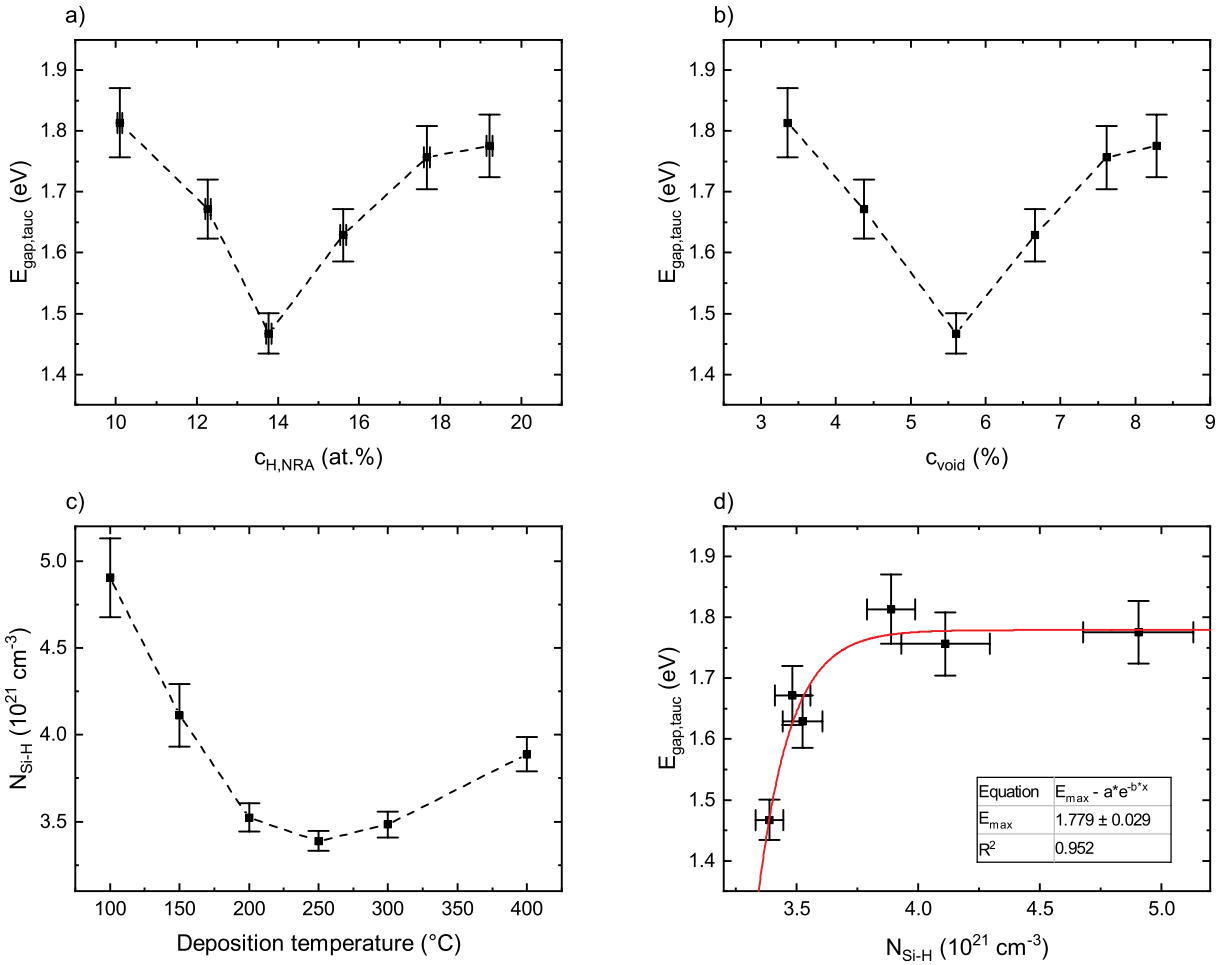

Fig. 5. a) Optical bandgap $E_{gap,tauc}$ as function of the NRA measured hydrogen concentration $c_{H,NRA}$ with local minimum, b) optical bandgap $E_{gap,tauc}$ as function of the microvoid volume fraction c_{void} with local minimum, c) Si-H bond density N_{Si-H} as function of the deposition temperature with local minimum, lines as guide for the eye. d) Optical bandgap $E_{gap,tauc}$ as function of the Si-H bond density N_{Si-H} without local minimum. Solid curve is exponential fit according to Eq. (11).

the optical bandgap of a-Si:H under variation of the deposition temperature, while the Si-H bond density describes this dependency alone. Therefore it is concluded, that the Si-H bond density is more appropriate for describing variations of the optical bandgap than the hydrogen concentration and the structural disorder. Following the hypothesis of a high Si-H bond density regime it is possible to explain previously published constant E_{gap} values under variation of the hydrogen concentration and structural disorder in [9,11].

Declaration of Competing Interest

The authors declare that they have no known competing financial interests or personal relationships that could have appeared to influence the work reported in this paper.

Acknowledgments

The authors like to thank Axel Herguth for specialized comments on the manuscript. Part of this work was financially supported by the German Federal Ministry of economic affairs and energy (FKZ 324042B).

References

[1] M. Stuckelberger, R. Biron, N. Wyrsch, F.-J. Haug, C. Ballif, Review: Progress in solar cells from hydrogenated amorphous silicon, Renew. Sust. Energ. Rev. 76 (2017) 1497–1523, https://doi.org/10.1016/j.rser.2016.11.190.
[2] G.D. Cody, T. Tiedje, B. Abeles, B. Brooks, Y. Goldstein, Disorder and the optical-absorption edge of hydrogenated amorphous silicon, Phys. Rev. Lett. 47 (1981) 1480–1483, https://doi.org/10.1103/PhysRevLett.47.1480.
[3] A.P. Sokolov, A.P. Shebanin, O.A. Golikova, M.M. Mezdrogina, Structural disorder and optical gap fluctuations in amorphous silicon, J. Phys. Condens. Matter 3 (1991) 9887–9894.
[4] S. Yamasaki, Optical absorption edge of hydrogenated amorphous silicon studied by photoacoustic spectroscopy, Philos. Mag. B 56 (1987) 79–97, https://doi.org/10.1080/13642818708211226.
[5] M. Daouahi, A. Ben Othmane, K. Zellama, A. Zeinert, M. Essamet, H. Bouchriha, Effect of the hydrogen bonding and content on the opto-electronic properties of radiofrequency magnetron sputtered hydrogenated amorphous silicon films, Solid State Commun. 120 (2001) 243–248, https://doi.org/10.1016/S0038-1098(01)00350-7.
[6] N. Maley, J.S. Lannin, Influence of hydrogen on vibrational and optical properties of a-Si1-xHx alloys, Phys. Rev. B 36 (1987) 1146–1152, https://doi.org/10.1103/PhysRevB.36.1146.
[7] S. Gupta, R.S.S. Katiyar, G. Morell, S.Z.Z. Weisz, The effect of hydrogen on the network disorder in hydrogenated amorphous silicon, Appl. Phys. Lett. 75 (1999) 2803–2805, https://doi.org/10.1063/1.125155.
[8] M. Yamaguchi, K. Morigaki, Effect of hydrogen dilution on the optical properties of hydrogenated amorphous silicon prepared by plasma deposition, Philos. Mag. B 79 (1999) 387–405, https://doi.org/10.1080/13642819908206415.
[9] M. Legesse, M. Nolan, G. Fagas, Revisiting the dependence of the optical and mobility gaps of hydrogenated amorphous silicon on hydrogen concentration, J. Phys. Chem. C 117 (2013) 23956–23963, https://doi.org/10.1021/jp408414f.
[10] E. Bertran, J.L. Andujar, A. Canillas, C. Roth, J. Serra, G. Sardin, Effects of deposition temperature on properties of r.f. glow discharge amorphous silicon thin films, Thin Solid Films 205 (1991) 140–145, https://doi.org/10.1016/0040-6090(91)90295-9.
[11] J. Müllerova, M. Fischer, M. Netrvalova, M. Zeman, P. Sutta, Influence of deposition temperature on amorphous structure of PECVD deposited a-Si:H thin films, Cent. Eur. J. Phys. 9 (2011) 1301–1308, https://doi.org/10.2478/s11534-011-0041-4.
[12] R.A. Street, Hydrogenated Amorphous Silicon, Cambridge University Press, Cambridge, 1991.
[13] J. Steffens, H.-W. Becker, S. Gerke, S. Joos, G. Hahn, B. Terheiden, Replacing NRA by fast GD-OES measurements as input to a model based prediction of hydrogen diffusion in a-Si, Energy Procedia 124 (2017) 180–187, https://doi.org/10.1016/j.egypro.2017.09.315.
[14] H.-W. Becker, D. Rogalla, Nuclear reaction analysis, in: H. Fritzsche, J. Huot, D. Fruchart (Eds.), Neutron Scatt. Other Nucl. Tech. Hydrog. Mater, Springer International Publishing, Switzerland, 2016, pp. 315–336, , https://doi.org/10.1007/978-3-319-22792-4.
[15] G.E. Jellison, F.A. Modine, Parameterization of the optical functions of amorphous materials in the interband region, Appl. Phys. Lett. 69 (1996) 371–373, https://doi.org/10.1063/1.118064.
[16] G.E. Jellison, F.A. Modine, Erratum: “Parameterization of the optical functions of amorphous materials in the interband region”, Appl. Phys. Lett. 69 (1996) 2137, https://doi.org/10.1063/1.118155.
[17] D.E. Aspnes, J.B. Theeten, F. Hottier, Investigation of effective-medium models of microscopic surface roughness by spectroscopic ellipsometry, Phys. Rev. B 20 (1979) 3292–3302, https://doi.org/10.1103/PhysRevB.20.3292.
[18] J. Tauc, R. Grigorovici, A. Vancu, Optical properties and electronic structure of amorphous germanium, Phys. Status Solidi 15 (1966) 627–637, https://doi.org/10.1002/pssb.19660150224.
[19] C. Manfredotti, F. Fizzotti, M. Boero, P. Pastorino, P. Polesello, E. Vittone, Influence of hydrogen-bonding configurations on the physical properties of hydrogenated amorphous silicon, Phys. Rev. B 50 (1994) 18046–18053, https://doi.org/10.1103/PhysRevB.50.18046.
[20] W. Liu, L. Zhang, F. Meng, W. Guo, J. Bao, J. Liu, D. Wang, Z. Liu, Characterization of microvoids in thin hydrogenated amorphous silicon layers by spectroscopic ellipsometry and Fourier transform infrared spectroscopy, Scr. Mater. 107 (2015) 50–53, https://doi.org/10.1016/j.scriptamat.2015.05.018.
[21] A.H.M. Smets, W.M.M. Kessels, M.C.M. van de Sanden, Vacancies and voids in hydrogenated amorphous silicon, Appl. Phys. Lett. 82 (2003) 1547–1549, https://doi.org/10.1063/1.1559657.
[22] G. Lucovsky, R.J. Nemanich, J.C. Knights, Structural interpretation of the vibrational spectra of a-Si:H alloys, Phys. Rev. B 19 (1979) 2064–2073, https://doi.org/10.1103/PhysRevB.19.2064.
[23] M. Cardona, Vibrational spectra of hydrogen in silicon and germanium, Phys. Status Solidi 118 (1983) 463–481, https://doi.org/10.1002/pssb.2221180202.
[24] H. Shanks, J. Fang, L. Ley, M. Cardona, F.J. Demond, S. Kalbitzer, Infrared spectrum and structure of hydrogenated amorphous silicon, Phys. Status Solidi 100 (1980), https://doi.org/10.1002/pssb.2221000103.
[25] J. Mouro, A. Gualdino, V. Chu, J.P. Conde, Microstructure factor and mechanical and electronic properties of hydrogenated amorphous and nanocrystalline silicon thin-films for microelectromechanical systems applications, J. Appl. Phys. 114 (2013) 184905, , https://doi.org/10.1063/1.4829020.
[26] U. Kroll, J. Meier, A. Shah, S. Mikhailov, J. Weber, Hydrogen in amorphous and microcrystalline silicon films prepared by hydrogen dilution, J. Appl. Phys. 80 (1996) 4971–4975, https://doi.org/10.1063/1.363541.
[27] J.C. van den Heuvel, M.J. Geerts, J.W. Metselaar, The relation between the optical properties and the hydrogen concentration in a-Si:H, Sol. Energy Mater. 22 (1991) 185–194, https://doi.org/10.1016/0165-1633(91)90016-E.
[28] Z. Remes, M. Vanecek, P. Torres, U. Kroll, A.H. Mahan, R.S. Crandall, Optical determination of the mass density of amorphous and microcrystalline silicon layers with different hydrogen contents, J. Non-Cryst. Solids 227–230 (1998) 876–879, https://doi.org/10.1016/S0022-3093(98)00207-5.
[29] A.H.H. Mahan, Y. Xu, D.L. Williamson, W. Beyer, J.D. Perkins, M. Vanecek, L.M. Gedvilas, B.P. Nelson, Structural properties of hot wire a-Si:H films deposited at rates in excess of 100 A/s, J. Appl. Phys. 90 (2001) 5038–5047, https://doi.org/10.1063/1.1407317.
[30] R.N. Kré, M.L. Moussé, Y. Tchétché, F.X.D. Bouo Bella, B. Aka, P.A. Thomas, Optical absorption of the hydrogenated evaporated amorphous silicon, Int. J. Phys. Sci. 5 (2010) 675–682.
[31] K. Zellama, L. Chahed, P. Sladek, M.L. Theye, J.H. von Bardeleben, P. Roca i Cabarrocas, Hydrogen-effusion-induced structural changes and defects in a-Si:H films: dependence upon the film microstructure, Phys. Rev. B 53 (1996) 3804–3812, https://doi.org/10.1103/PhysRevB.53.3804.
[32] K. Fukutani, M. Kanbe, W. Futako, B. Kaplan, T. Kamiya, C.M. Fortmann, I. Shimizu, Band gap tuning of a-Si:H from 1.55 eV to 2.10 eV by intentionally promoting structural relaxation, J. Non-Cryst. Solids 227–230 (1998) 63–67, https://doi.org/10.1016/S0022-3093(98)00022-2.